IEEE Photonics Journal
An IEEE Photonics Society Publication

Open Access

A Low-Cost and High-Wavelength-Precision Fabrication Method for Multiwavelength DFB Semiconductor Laser Array

Volume 6, Number 3, June 2014

Yuechun Shi
Rui Liu
Shengchun Liu
Xiaojun Zhu

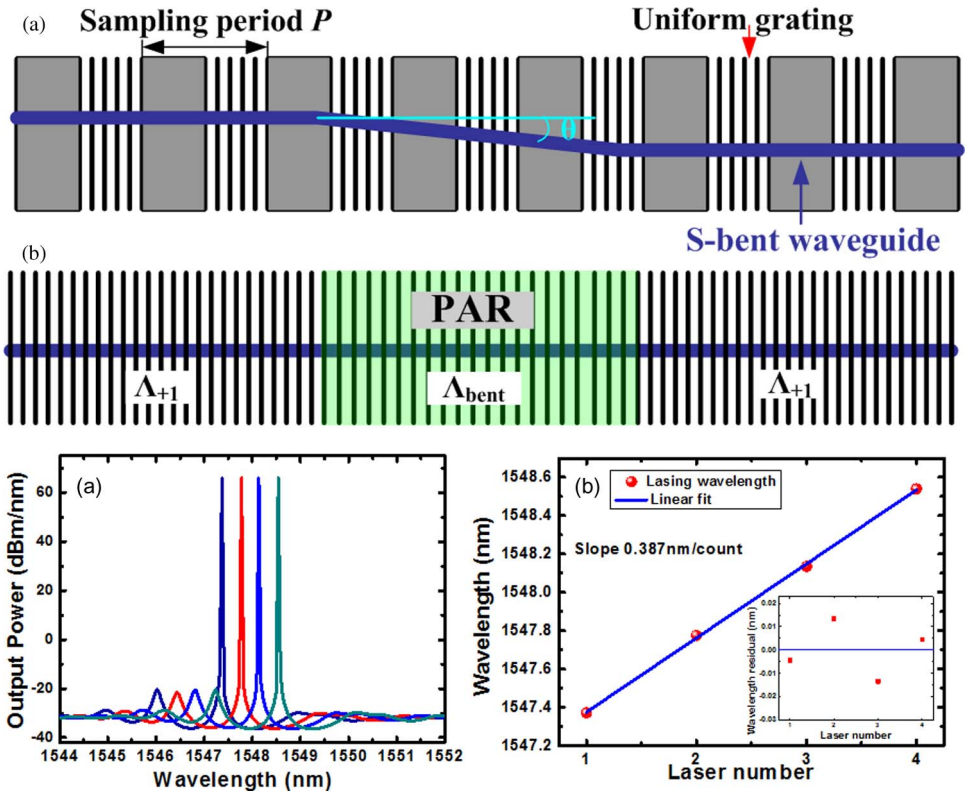

DOI: 10.1109/JPHOT.2014.2317674
1943-0655

A Low-Cost and High-Wavelength-Precision Fabrication Method for Multiwavelength DFB Semiconductor Laser Array

Yuechun Shi,[1] Rui Liu,[1] Shengchun Liu,[1,2] and Xiaojun Zhu[3]

[1]National Laboratory of Solid State Microstructures, Microwave-Photonics Technology Laboratory, College of Engineering, and Applied Sciences, Nanjing University, Nanjing 210093, China
[2]College of Physical Science and Technology, Heilongjiang University, Harbin 150080, China
[3]The School of Electronic and Information, Nantong University, Nantong 226000, China

DOI: 10.1109/JPHOT.2014.2317674

Manuscript received February 15, 2014; revised March 31, 2014; accepted April 1, 2014. Date of publication April 15, 2014; date of current version May 5, 2014. This work was supported in part by the National Natural Science Foundation of China under Grant 11274099, by the National Natural Science Foundation for the Youth under Grant 61306068, by the Natural Science Foundation of Jiangsu Province of Youth under Grant BK20130585, by the High Level Innovation Teams of Heilongjiang University under Grant HD-028, by the Natural Science Foundation of Jiangsu Province of China under Grant SBK201341292, and by the Science and Technology Program of Nantong under Grant BK2013042. Corresponding author: S. Liu (e-mail: shengchunliu@163.com).

Abstract: A new method to fabricate the multiwavelength DFB semiconductor laser array (MLA) is proposed for the first time based on sampled grating and s-bent waveguide. According to the detailed precision analysis, the lasing wavelength accuracy of the proposed structure is significantly improved. Because the common holography exposure and micrometer photolithography are used to fabricate the sampled grating and the bent waveguide in this method, the fabrication cost is very low. Therefore, it offers a suitable method for massive fabrication.

Index Terms: Sampled grating, bent waveguide, DFB laser, laser array.

1. Introduction

The integrated multiwavelength DFB semiconductor laser array (MLA) is one of the most important elements in the photonic integrated circuits (PICs) [1]–[3]. For practical applications, accurate lasing wavelength of laser array is required to meet the ITU-T standard. With the increase of the channel number in the dense Wavelength Division Multiplex (DWDM) system, the wavelength spacing between two adjacent lasers becomes smaller and smaller, such as from 0.8 nm to 0.4 nm. Thus, each lasing wavelength needs to be controlled precisely. So the massive fabrication of such array is still a problem. Up to now, the most commonly used method is the electron beam lithography (EBL) [1], [4]. It can accurately write the grating line by line to generate the complex grating patterns. But it is time consuming as well as of high cost. Besides, it is also limited by finite writing field and vulnerability to outside influences such as the temperature variation and vibration [5]. So it is still a challenge for EBL to exactly control wavelength spacing of two adjacent lasers. Therefore, the additional wavelength tuning is usually required in actual applications [6], [7]. Some other methods are also proposed to fabricate the MLA, such as the asymmetric sampled grating, bent waveguide and varied waveguide width [3], [8], [9]. But both methods of bent waveguide and the varied waveguide width have very limited lasing wavelength range and are also lack of uniformities due to

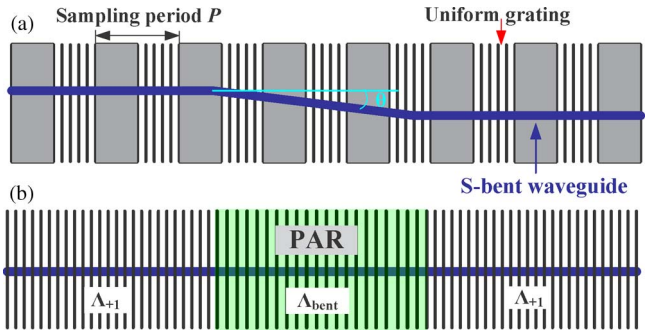

Fig. 1. The schematic of (a) the proposed structure and (b) the grating pattern in +1st subgrating.

the different waveguide structures of each laser. As a result, it is hard to simultaneously realize flexibility, reliability and low cost with both methods.

In this paper, a new method is proposed to fabricate the MLA with low cost and high wavelength precision. A wide range of lasing wavelength can be realized by changing the sampling period. Meanwhile, the single longitudinal mode (SLM) operation can be ensured by pre-designing S-bent waveguide. The sampled grating can be fabricated by the common holography exposure and the bent waveguide only needs conventional μm-*level photolithography*. So the cost is very low. According to the detailed theoretical analysis, the wavelength precision is high. Therefore it is a promising way to realize the MLA with high wavelength precision and low cost fabrication.

2. Principle and Theoretical Analysis

2.1. Principle

According to the Fourier analysis, the sampled grating as shown in Fig. 1(a) can be expressed as [10]

$$\Delta n(z) = \frac{1}{2}\Delta n_s \sum_m F_m \exp\left[j\left(2\pi\frac{z}{\Lambda_0} + 2m\pi\frac{z}{P}\right)\right] + c.c \tag{1}$$

where P is the sampling period; Λ_0 is the period of the basic grating (seed grating); Δn_s is the index modulation of the seed grating; m denotes the mth order Fourier series and F_m is the Fourier coefficient of the mth subgrating. If the +1st order subgrating is used as filter, the relation between the seed grating and the sampling period can be expressed as

$$\frac{1}{\Lambda_{+1}} = \frac{1}{\Lambda_0} + \frac{1}{P}. \tag{2}$$

Therefore, the Bragg wavelength of +1st subgrating can be changed by sampling period P as shown in Fig. 2(a) which is simulated by Transfer Matrix Method (TMM) [11].

In addition, the grating period in the bent waveguide region can be expressed as

$$\Lambda_{\text{bent}} = \frac{\Lambda_{+1}}{\cos\theta} = \frac{\Lambda_0 P}{(P+\Lambda_0)\cos\theta}. \tag{3}$$

Here, θ is the tilted angle of the bent waveguide. Therefore, the grating period in the bent waveguide region is determined by θ, sampling period P and seed grating period Λ_0 as shown in Fig. 1(b). It should be mentioned that the sampling period along bent waveguide is also slightly changed by tilted angle as shown in Fig. 3.

Because Λ_{bent} is larger than Λ_{+1}, a continuous phase change in grating can be induced in the bent waveguide region, which is also called phase adjust region (PAR), i.e., corrugated pitch

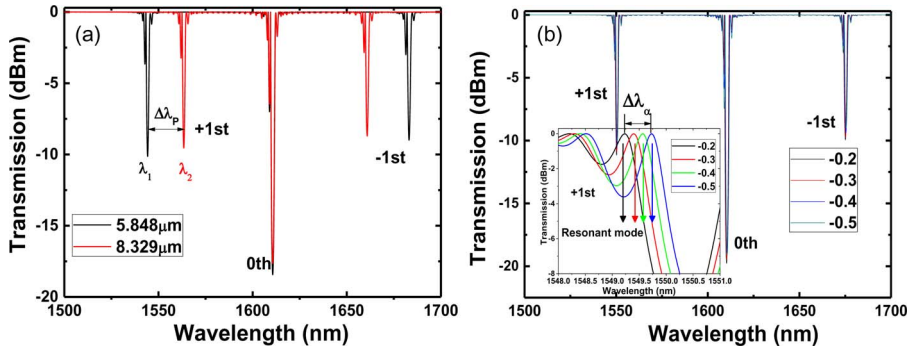

Fig. 2. The transmission spectra with (a) different sampling period P and (b) same P but different α.

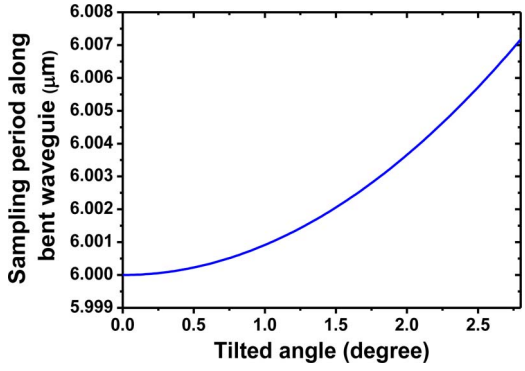

Fig. 3. The relation between sampling period along the bent waveguide and tilted angle. Here, the actual sampling period is 6 μm.

modulation (CPM) [12], [13]. We further express this phase change as follows:

$$\frac{L_2}{\Lambda_{\text{bent}}} - \frac{L_2}{\Lambda_{+1}} = \alpha. \tag{4}$$

Here α is a phase change coefficient which indicates the phase change of the PRA comparing with the uniform grating. A resonant mode can be created by tilted waveguide. For example, when $\alpha = -0.5$, a π phase shift is introduced. Furthermore, it also indicates that different tilted angles can cause different values of α or phase change value from Eqs. (3) and (4). Because the relative resonant wavelength within grating stop-band is determined by phase change value, there is a slight resonant wavelength variation still caused by tiled angle though the sampling period, and the seed grating period are fixed. As shown in Fig. 2(b), we simulated the transmission spectra with α from -0.2 to -0.5. The Bragg wavelength of all the subgratings keeps the same, but the resonant mode wavelengths are different as shown in the inserted figure of Fig. 2(b). The variation range $\Delta\Lambda_\alpha$ is about 0.48 nm.

As a result, for a MLA, the coarse lasing wavelength with large wavelength range of each laser can be controlled by the sampling period P and Λ_0 according to Eq. (2). But the fine wavelength is controlled by the tilted angle or value of α. In addition, according to Eqs. (3) and (4), θ is usually small. For example, it is only 2.44 degrees when sampling period is 6.498 μm for $+1$st Bragg wavelength of 1550 nm and α is -0.5. Because of the bent structure, the radiation loss can happen in the joint section. So we simulated the radiation loss by 3-dimensional Beam Propagation Method (3D-BPM). The cross section is the common ridge structure for DFB lasers as shown in Fig. 4(a). The transmissions of the joint section with tilted angles from 1.0 to 2.8 degrees are shown in

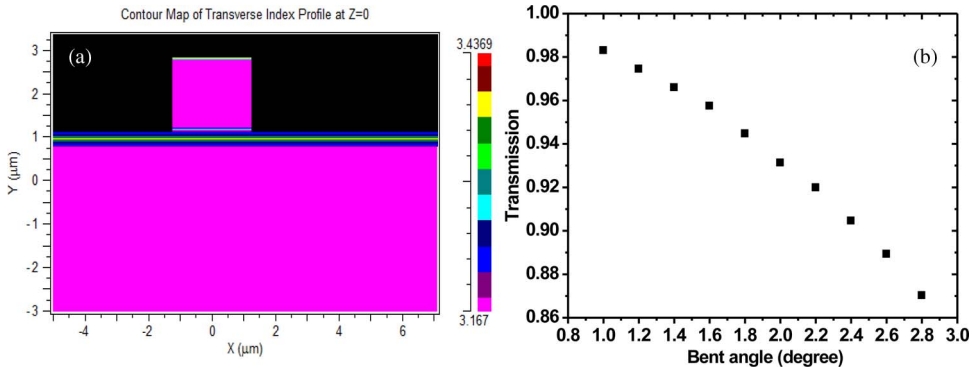

Fig. 4. (a) The index profile of the cross section of the ridge waveguide. (b) The calculated transmissions of the bent waveguide at different tilted angles.

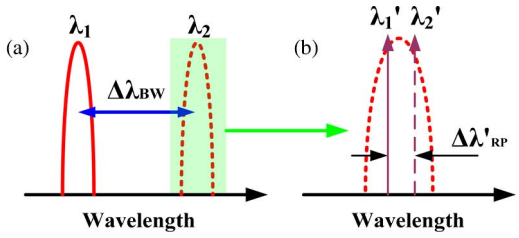

Fig. 5. The schematic of two main wavelength deviations with (a) BW-error and (b) RP-error. Here, λ_1 and λ_2 are the Bragg wavelengths, and λ_1' and λ_2' are the resonant wavelengths with the same Bragg wavelength.

Fig. 4(b). So the tilted angle should be as small as possible if SLM operation is ensued. Finally, the DFB laser array with SLM operation can be achieved by changing the sampling period and introducing a small tilted angle in the waveguide. Because the seed grating is uniform, the fabrication of the proposed structure only needs the low cost holography exposure and the common μm-level photolithography.

2.2. Precision Analysis

The error of the lasing wavelength is mainly caused by two reasons, including Bragg wavelength error (BW-error) $\Delta\lambda_{BW}$ and the relative wavelength error of lasing mode in stop-band (RP-error) $\Delta\lambda'_{RP}$ as shown in Fig. 5. The BW-error $\Delta\lambda_{BW}$ mainly comes from the errors of the effective refractive index and the grating period. As an example and indicated in Fig. 2(a), the sampling period change or error can lead to the wavelength shift of the stopband of $\pm$1st subgrating. The RP-error is usually caused by the error of the resonant phase conditions such as the different phase shifts in the PAR of the grating and the random grating phase caused by the cavity facet. As indicated in Fig. 2(b), there is a wavelength shift caused by grating phase variation if the value of α is changed by some reasons such as error in fabrication. So the total error $\Delta\lambda$ of the lasing wavelength can be expressed as

$$\Delta\lambda = \Delta\lambda_{BW} + \Delta\lambda'_{RP}. \tag{5}$$

2.2.1. BW-Error

For the BW-error, the variation of the effective refractive index only leads to the same wavelength shift for all lasing wavelengths of array. So only the error of the grating period is considered here,

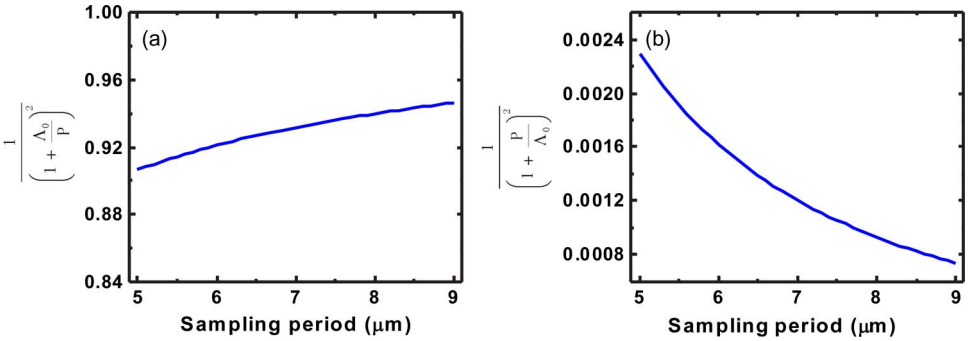

Fig. 6. (a) Seed grating error coefficient for different sampling periods. (b) Sampling period error coefficient for different sampling periods (seed grating period is 251.56 nm).

which can be expressed as

$$d\Lambda_{+1} = \frac{1}{\left(1+\frac{\Lambda_0}{P}\right)^2} d\Lambda_0 + \frac{1}{\left(1+\frac{P}{\Lambda_0}\right)^2} dP. \tag{6}$$

Because the seed grating error is nearly the same for the different sampling period P as shown in Fig. 6(a). So the wavelength spacing still maintains the same for a MLA. As a result, this error can be neglected.

For the sampling period error, the error coefficient is shown in Fig. 6(b). When sampling period is 6 μm and error ΔP is about 50 nm, this error is only around 0.08 nm which corresponds to the Bragg wavelength shift of 0.512 nm. So the error induced by sampling period is also small.

2.2.2. RP-Error

According to Eq. (4), the lasing wavelength error of the grating phase variation is related to the value of α, so its error is directly related to $\Delta\lambda'_{RP}$ and can be expressed as

$$d\alpha = (1-\cos\theta)\frac{L_2}{\Lambda_{+1}^2} d\Lambda_{+1} - \frac{L_2}{\Lambda_{+1}} \sin\theta d\theta. \tag{7}$$

Considering the first part in Eq. (7), substitute Eqs. (3) and (4) into this part, and we get

$$(1-\cos\theta)\frac{L_2}{\Lambda_{+1}^2} d\Lambda_{+1} = -\frac{\alpha}{\Lambda_{+1}} \left[\frac{1}{\left(1+\frac{\Lambda_0}{P}\right)^2} d\Lambda_0 + \frac{1}{\left(1+\frac{P}{\Lambda_0}\right)^2} dP \right]. \tag{8}$$

For term of the error induced by the sampling period $-(\alpha/\Lambda_{+1})(1/(1+(P/\Lambda_0))^2)dP$, P is larger than an order of magnitude. So the error induced by sampling period is very small, and thus can be neglected.

For term of the error induced by seed grating $-(\alpha/\Lambda_{+1})(1/(1+(\Lambda_0/P))^2)d\Lambda_0$, the error is decreased by $(1/(1+(\Lambda_0/P))^2)$ compared with the normal grating structure. Because $(1/(1+(\Lambda_0/P))^2)$ approaches to 1 and the value of α/Λ_{+1} is small, the magnification of $(\alpha/\Lambda_{+1})(1/(1+(P/\Lambda_0))^2)$ is also very small. For example, when Λ_{+1} is 242 nm and an error of 1.0 nm in seed grating can only lead to an error of 0.002 in α. So based on the above discussions, the proposed method has much smaller error induced by grating comparing with normal grating structures.

And then, we discuss the second part in Eq. (7). The error induced by tilted angle of $(L_2/\Lambda_{+1})\sin\theta d\theta$ is usually caused by the tilt of the wafer or the wafer holder during the photolithography of the waveguide. The value of θ is usually small which is usually equal to only $1 \sim 3^\circ$ if

α is -0.5. For the current fabrication technology, the deviation of tilted angle $\Delta\theta$ can be very small. So its influence on the lasing wavelength error is also very small accordingly. Besides, for the different grating periods Λ_{+1} of the different lasers in the array, if the tilted angle deviations on the same wafer are nearly the same, thus deviation of α induced by this error is nearly the same as well according to second part in Eq. (7). For example, if lasing wavelength is 1570 nm, the coefficient is 14.226. For 1530-nm lasing wavelength, this coefficient is 14.598. Here, $\theta = 2^\circ$, $n_{\text{eff}} = 3.2$ and $L_2 = 100$ μm are used. This means that the tilted angle error induced by the tilt of the wafer or the wafer holder is nearly the same for all lasers in array. In other words, the lasing wavelength spacing of the array will keep nearly invariant. In the practical application, the precise wavelength spacing of the laser array, which should obey the ITU-T standard, is more important than the whole absolute wavelength. As a result, the angle error can be ignored according to the above analysis.

2.3. Design of Multiwavelength DFB Laser Array

For designing an MLA, the Bragg wavelength of grating can be easily controlled by sampling period. But it only determines the course lasing wavelength as shown in Fig. 2(a). For the specific resonant wavelength within the stopband shown in Fig. 2(b), the tilted angle should be carefully designed, that is, how to get a fixed α for each laser exactly. According to Eqs. (3) and (4), we can further obtain that

$$\cos\theta = \frac{\alpha\Lambda_{+2}}{L_2} + 1 \tag{9}$$

$$d\theta = -\frac{\alpha}{L_2 \sin\theta} d\Lambda_{+1}. \tag{10}$$

Assuming L_2, Λ_{+1} and θ are 133.3 μm, 242.2 nm, 2.44 degrees, respectively. Laser cavity is 400 μm. Therefore, $\alpha/L_2\sin\theta$ is about $8.8 * 10^{-5}$ (radian/nm). It means the tilted angle difference among different lasers in array is rather small. For example, if 20-nm lasing wavelength spacing is required, the grating period variation is about 3.125 nm, assuming the effective index is 3.2. The tilted angle difference is only 0.0157 degrees accordingly. On the other hand, according to Eq. (7), the error of α induced by tilted angle error θ is also very small in case θ and $\Delta\theta$ is small. So the angle difference of 0.0157 degrees only leads to the variation of α around 0.0064. Therefore, in the actual design, the tilted angle can be kept as the same value for lasers with different wavelengths.

3. Simulation Results and Discussions

3.1. Simulation Results

A single DFB laser with proposed grating structure is studied first. The characteristics of the corresponding passive grating resonator are simulated. The transmission spectrum with α of -0.5 is shown in Fig. 2(b). If $+1$st subgrating is used as resonator, a resonant mode around 1550 nm can be formed. Furthermore, the DFB laser with the same grating structure is also simulated by TMM method [14]. The TMM method is based on the coupled mode theory. The spatial hole burning effect is also included [15]. It can precisely simulate the lasing wavelength. However the thermal effect is not included. But it does not affect the wavelength precision because it is well known that the wavelength shift ratio of each laser is nearly the same when the same material is used and the value is about 0.09 nm/$^\circ$C for InP-based materials [16], [17].The main parameters are listed in the Table 1. Since the length is increased by bent structure, in order to keep the whole virtual optical cavity length to 400 μm, the bent waveguide along horizontal direction should be shorter than the straight waveguide. Therefore, the device length (laser length along horizontal direction) is also a little shorter than 400 μm. Because the 0th channel resonance is about 1610 nm, which is far away from the gain region, it can avoid potential lasing. If the $+1$st

TABLE 1

Basic parameters in the simulation

Cavity length (L)	400 μm
Seed grating period (Λ_0)	251.56nm
Normalized coupling coefficient of +1st sub-grating (κL)	2.0
Length of PRA (L_{bent})	133μm
Effective refractive index (N_{eff})	3.2
Slope of gain-carrier density relationship (a)	2.0×10^{-16} cm^2
Transparency carrier density (N_t)	1.2×10^{18} cm^{-3}
Confinement factor (Γ)	0.3
Linewidth enhancement factor (β)	1.5
Linear carrier lifetime (τ)	4ns
Waveguide loss (α)	30 cm^{-1}
Active layer thickness (d)	180nm

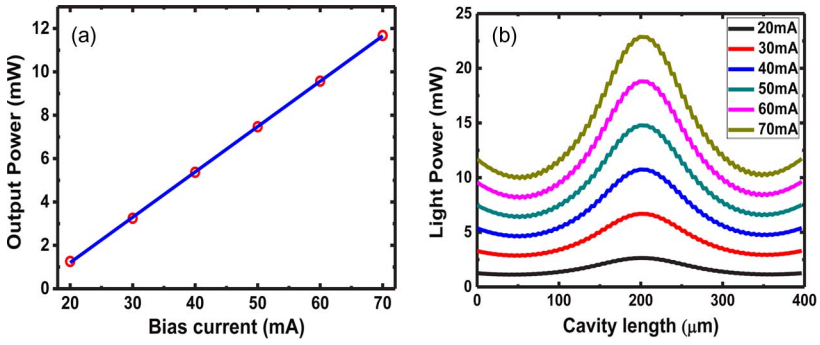

Fig. 7. The calculated curves of (a) P–I curve of the proposed laser and (b) the internal light intensity distribution along cavity under different injection currents.

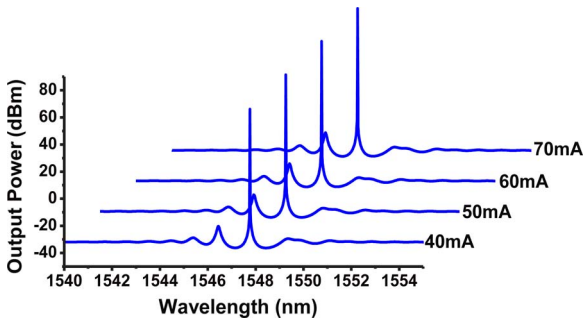

Fig. 8. The simulated lasing spectra of the proposed laser at bias current of 40 mA, 50 mA, 60 mA, and 70 mA, respectively.

subgrating is used, single longitudinal mode (SLM) can be ensured. As shown in Fig. 7(a), the Power–Current (P–I) curve is simulated. The threshold current is about 14.2 mA, and the slope efficiency is about 0.21 WA^{-1} by linear fit. The internal light intensity distributions along cavity at different bias currents are given in Fig. 7(b). The lasing spectra at different currents are also simulated and shown in Fig. 8.

As an example, we also designed a four-wavelength DFB laser array with wavelength spacing of 6.4 nm, which leads to about 25-nm wavelength coverage of the MLA to verify the effectiveness in

TABLE 2

Some parameters related to lasing wavelength of the array with 6.4-nm wavelength spacing

Laser number	Sampling period (μm)	+1st sub-grating period(nm)	Accurate tilted angle according to Eq.10(degree)	Tilted angle used in simulation (degree)	Bragg wavelength of the +1st sub-grating (nm)	Lasing wavelength (thermal effect is not included) at 40mA (nm)
1	5.848	241.188	2.437	2.44	1549.6	1541.33
2	6.499	242.188	2.442	2.44	1550.0	1547.76
3	7.305	243.188	2.447	2.44	1556.4	1554.12
4	8.329	244.188	2.452	2.44	1562.8	1560.50

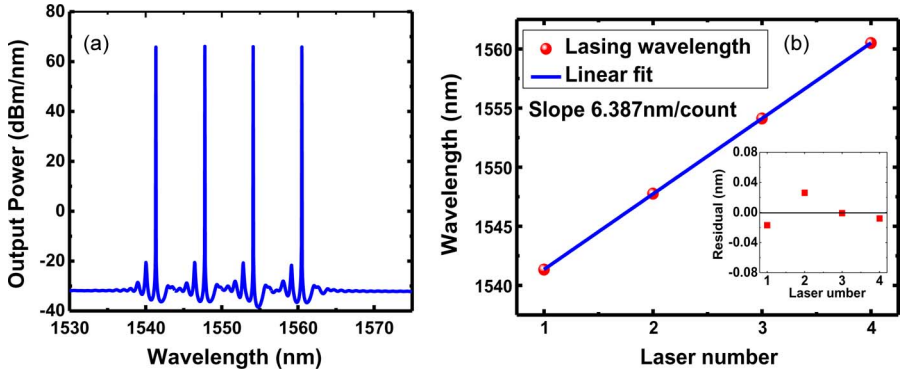

Fig. 9. (a) The simulated lasing spectra of the four-wavelength array with designed lasing wavelength spacing of 6.4 nm at bias current of 40 mA. (b) The simulated lasing wavelengths and their linear fit; the inserted figure is the wavelength residual after linear fit.

TABLE 3

Some parameters related to lasing wavelength of the array with 0.4-nm wavelength spacing

Laser number	Sampling period (μm)	+1st sub-grating period(nm)	Accurate tilted angle according to Eq.10(degree)	Tilted angle used in simulation (degree)	Bragg wavelength of the +1st sub-grating (nm)	Lasing wavelength (thermal effect is not included) at 40mA (nm)
1	6.453	242.125	2.44178	2.44	1549.6	1547.370
2	6.499	242.188	2.44209	2.44	1550.0	1547.775
3	6.544	242.250	2.44241	2.44	1550.4	1548.135
4	6.589	242.3125	2.44272	2.44	1550.8	1548.540

case of large wavelength range. Some parameters used in simulation and related to lasing wavelength are shown in Table 2. The bias current is 40 mA. All the lasers share the same seed grating with period of 251.56 nm. The waveguide tilted angles are all 2.44 degrees to verify the analysis in Section 2.3.

Fig. 9(a) is the simulated spectra of the four-wavelength DFB laser array, and the lasing wavelengths are plotted in Fig. 9(b). The relative error of the wavelength slope after linear fit is 0.20%. Good wavelength uniformity is obtained. We also simulated a four-wavelength array with wavelength spacing of 0.4 nm. Table 3 shows some parameters used in simulation and related to the lasing wavelength of the array. Fig. 10(a) is the simulated lasing spectra. The corresponding lasing wavelengths are shown in Fig. 10(b). Good wavelength accuracy is also obtained here.

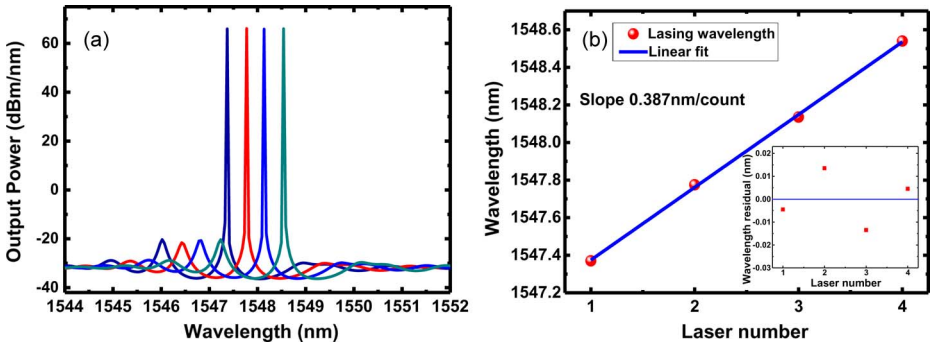

Fig. 10. (a) The simulated lasing spectra of the four-wavelength array with designed lasing wavelength spacing of 0.4 nm at bias current of 40 mA. (b) The simulated lasing wavelengths and their linear fit; the inserted figure is the wavelength residual after linear fit.

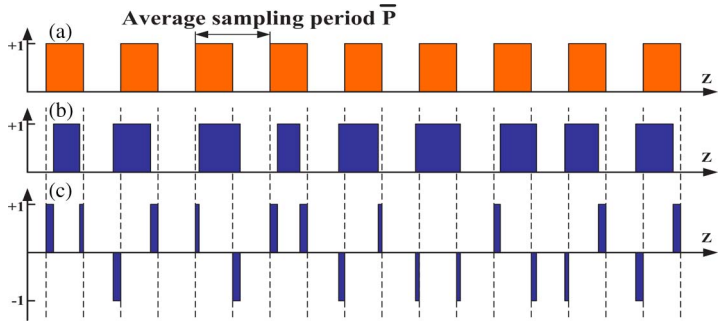

Fig. 11. The schematic of the error in sampling pattern with (a) the ideal sampling pattern with uniform sampling period, (b) the sampling pattern errors on photomask, and (c) the residual random pulse series compared with (a).

3.2. Discussion

According to current fabrication technology for photomask, it is easy to control the error of the line on photomask into 0.1 μm, but during the process of photolithography for sampling pattern, it is impossible to exactly transfer the pattern on photomask into wafer for the reasons such as the lateral etch and exposure light diffraction, but these defects only change the duty cycle on the wafer and do not affect the sampling period at all. According to above analysis, the lasing wavelength is only affected by sampling period. Therefore, the high precision of wavelength still can be ensured under the conditions of the imperfect processes described above.

On the other hand, Eq. (6) considers the worst case. That is, each sampling period deviates the same value and in the same direction. This situation can be considered as the system error. If every laser in array has the same error, the whole wavelength grid will shift slightly. But the wavelength spacing probably maintains the same. In this case, this error nearly can be ignored. Furthermore, if each sampling period error, which may be caused by mask fabrication for example, is independent but follows the same probability distribution such as the Gaussian distribution, the situation will be quite different. As shown in Fig. 11, the real sampling pattern can be considered as the superposition of an ideal sampling pattern with uniform sampling period of $\overline{P}$ shown in Fig. 11(a) and a random pulse series shown in Fig. 11(c). Here, $\overline{P}$ is the average sampling period when sampling pattern is fabricated. Furthermore, it can be expressed as

$$\Delta n(z) = \frac{1}{2}\Delta n S^{\text{real}}(z)\left[\exp\left(j\frac{2\pi}{\Lambda_0}z\right) + c.c\right]. \tag{11}$$

Here, $S^{\text{real}}(z)$ denotes the real sampling pattern. Therefore, it can be further divided into two parts: $S^{\text{uniform}}(\overline{P})$, which denotes uniform sampling pattern with period of $\overline{P}$ and fabrication error function $Error(z)$, which is considered as random pulse series. So it can be expressed as

$$S^{\text{real}}(z) = S^{\text{uniform}}(\overline{P}) + Error(z). \tag{12}$$

$Error(z)$ can be further expressed as [18]

$$Error(z) = \sum_{n=0}^{N-1} \text{sign}(\omega_n)\Pi\left[\frac{z - \left(n\overline{P} + \frac{\omega_n}{2}\right)}{|\omega_n|}\right] + \sum_{j=0}^{N-1} \text{sign}(\nu_j)\Pi\left[\frac{z - \left(j\overline{P} + \frac{\overline{p}}{2} - \frac{\nu_j}{2}\right)}{|\nu_j|}\right]. \tag{13}$$

Here, N is the sampling period number, and $\Pi(z - z_0/|\omega|)$ is rectangle function with width of ω and center of Z_0. ω_n and ν_j are the random numbers with mean value of zero.

For weekly modulated index grating, the reflection spectrum is related to its Fourier transform, which can be expressed as [19]

$$\Re(\beta) \propto \left| F\left[\frac{1}{2}\Delta n S^{\text{real}}(z)\left[\exp\left(j\frac{2\pi}{\Lambda_0}z\right) + \text{c.c}\right]\right]\right|^2. \tag{14}$$

Here, β is $2\pi n_{eff}\lambda^{-1}$, and F denotes the Fourier transform. Then, Eq. (14) can be further expressed as

$$\Re(\beta) \propto \left| F^{\text{uniform}}\left\{\frac{1}{2}\Delta n S^{\text{uniform}}(\overline{P})\left[\exp\left(j\frac{2\pi}{\Lambda_0}z\right) + \text{c.c}\right]\right\} + F^{\text{random}}\left\{\frac{1}{2}\Delta n Error(z)\left[\exp\left(j\frac{2\pi}{\Lambda_0}z\right) + \text{c.c}\right]\right\}\right|^2. \tag{15}$$

From Eq. (15), we can see that the reflection spectrum of the sampled grating with error is a superposition of the reflectance of ideal sampled grating and a random pulsed series. Since the component of ideal sampled grating is uniform, it leads to intensive reflectance. The error induced reflectance F^{random} can broaden the whole reflection bandwidth because it leads to a wider frequency range [15], but the Bragg wavelength is still determined by ideal sampled grating F^{uniform} for its intensive interaction with light. In other words, the Bragg wavelengths of subgratings are only determined by the average sampling period of $\overline{P}$.

According to central-limit theorem in probability theory, $\overline{P} - \mu/(\sigma/\sqrt{N})$ follows the Gauss distribution and can be expressed as

$$\frac{\overline{P} - \mu}{\sigma/\sqrt{N}} \sim \text{Gauss}(\mu, \sigma^2/N). \tag{16}$$

As an example, if the sampling period distribution of $P(z)$ has expectation μ of 6 μm, which is the exact sampling period we want, and standard deviation σ of 50 nm. So N, which is the sampling number, is about 66 for a 400-μm-long cavity. Then, standard deviation of $\overline{P}$ is $\sigma/\sqrt{N}$ whose value is only 6.15 nm. The precision is further improved greatly comparing with Eq. (6).

We simulated the transmission spectra of the sampled gratings with ideal uniform sampling pattern and with random errors in sampling pattern respectively. The half sampling periods are 3000 nm and 3010 nm for ideal sampling patterns, and the mean half sampling periods are 2997.20 nm and 3008.09 nm for those with random error. All the other parameters are the same. As shown in Fig. 12(a), except the grating with ideal half sampling period of 3100 nm, the other three spectra of the +1st subgrating are nearly overlapped with reflection peak of around 1545.2 nm. Fig. 12(b) shows the half sampling period distribution with random error and mean value of

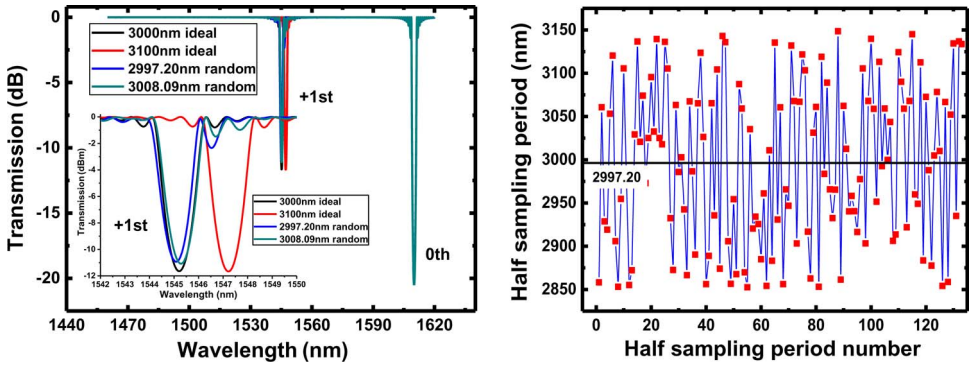

Fig. 12. (a) The transmission spectra of the sampled grating with ideal sampling structure (3000-nm half sampling period), the sampling structures with random error (2997.20-nm and 3008.09-nm mean half sampling period), and ideal sampling structure (3100-nm half sampling period). (b) The half sampling periods along cavity with random error.

2997.20 nm along cavity. Then, the half sampling periods are from 2850 nm to 3150 nm with variation of $\pm$150 nm. However, supposing that the sampling pattern is also ideal and its half period is 3100 nm, the reflection peak of $+$1st subgrating is 1547.22 nm, and there is around 2.0-nm wavelength deviation, which is much larger than the one with ideal half period of 3000 nm, as shown in Fig. 12(a). The results are consistent with the above theoretical analysis.

4. Conclusion

A new method to fabricate MLA is proposed. The detailed precision analysis is also given. High wavelength precision can be obtained according to theoretical analysis. Because only the uniform grating and μm-level sampling pattern are required and the resonant mode is caused by bent waveguide, only the common holographic exposure and μm-level photolithography is used. So the cost of fabrication is very low. This method may be a promising way for the future high count MLA for PICs.

References

[1] T.-P. Lee *et al.,* "Multiwavelength DFB laser array transmitters for ONTC reconfigurable optical network testbed," *J. Lightwave Technol.*, vol. 14, no. 6, pp. 967–976, Jun. 1996.
[2] Y. Sasahata *et al.,* "Tunable DFB laser array integrated with Mach–Zehnder modulators for 44.6 Gb/s DQPSK transmitter," *IEEE J. Sel. Topic Quantum Electron.*, vol. 19, no. 4, p. 1501507, Jul./Aug. 2013.
[3] S.-W. Ryu, S.-B. Kim, J.-S. Sim, and J. Kim, "Monolithic integration of a multiwavelength laser array associated with asymmetric sampled grating lasers," *IEEE J. Sel. Topic Quant. Electron.*, vol. 8, no. 6, pp. 1358–1365, Nov./Dec. 2002.
[4] T. Kjellberg, S. Nilsson, T. Klinga, B. Broberg, and R. Schatz, "Investigation on the spectral characteristics of DFB lasers with different grating configurations made by electron-beam lithography," *J. Lightw. Technol.*, vol. 11, no. 9, pp. 1405–1415, Sep. 1993.
[5] T. Kjellberg and R. Schatz, "The effect of stitching errors on the spectral characteristics of DFB lasers fabricated using electron beam lithography," *J. Lightw. Technol.*, vol. 10, no. 9, pp. 1256–1266, Sep. 1992.
[6] J. Zhao *et al.,* "Experimental demonstration of a 16-channel DFB laser array based on nanoimprint technology," *Semicond. Sci. Technol.*, vol. 28, no. 5, pp. 1–6, 2013.
[7] I.-F. Jang and S.-L. Lee, "Simple approaches of wavelength registration of monolithically integrated DWDM laser arrays," *IEEE Photon. Technol. Lett.*, vol. 14, no. 12, pp. 1659–1661, Dec. 2002.
[8] H. Hillmer and B. Klepser, "Low-cost edge-emitting DFB laser arrays for DWDM communication systems implemented by bent and tilted waveguides," *IEEE J. Quantum Electron.*, vol. 40, no. 10, pp. 1377–1383, Oct. 2004.
[9] G. P. Li, T. Makino, and C. M. Wu, "Multi-λ ridge waveguide gain-coupled DFB laser array," *J. Lightw. Technol.*, vol. 13, no. 2, pp. 196–199, Feb. 1995.
[10] J. Li *et al.,* "Experimental demonstration of distributed feedback semiconductor lasers based on reconstruction-equivalent-chirp technology," *Opt. Exp.*, vol. 17, no. 7, pp. 5240–5245, Mar. 2009.
[11] M. Yamada and K. Sakuda, "Analysis of almost-periodic distributed feedback slab waveguide via a fundamental matrix approach," *Appl. Opt.*, vol. 26, no. 16, pp. 3474–3478, Aug. 1987.

[12] W. Li, X. Zhang, and J. Yao, "Experimental demonstration of a multi-wavelength distributed feedback semiconductor laser array with an equivalent chirped grating profile based on the equivalent chirp technology," *Opt. Exp.*, vol. 21, no. 17, pp. 19 966–19 971, Aug. 2013.
[13] Y. Dai and J. Yao, "Numerical study of a DFB semiconductor laser and laser array with chirped structure based on the equivalent chirp technology," *IEEE J. Quantum Electron.*, vol. 44, no. 10, pp. 938–945, Oct. 2008.
[14] G. P. Agrawal and A. H. Bobeck, "Modeling of distributed feedback semiconductor lasers with axially-varying parameters," *IEEE J. Quantum Electron.*, vol. 24, no. 12, pp. 2407–2414, Dec. 1988.
[15] W. Fang, A. Hsu, S. L. Chuang, T. Tanbun-Ek, and A. M. Sergent, "Measurement and modeling of distributed-feedback lasers with spatial hole burning," *IEEE J. Sel. Topic Quantum Electron.*, vol. 3, no. 2, pp. 547–554, Apr. 1997.
[16] Y. Shi *et al.,* "Experimental demonstration of the three phase shifted DFB semiconductor laser based on reconstruction-equivalent-chirp technique," *Opt. Exp.*, vol. 20, no. 16, pp. 17 374–17 379, Jul. 2012.
[17] Y. Shi *et al.,* "Study of the multiwavelength DFB semiconductor laser array based on the reconstruction-equivalent-chirp technique," *J. Lightw. Technol.*, vol. 31, no. 20, pp. 3243–3250, Oct. 2013.
[18] G. Coppola, A. Irace, A. Cutolo, and M. Lodice, "Effect of fabrication errors in channel waveguides Bragg gratings," *Appl. Opt.*, vol. 38, no. 9, pp. 1752–1758, Mar. 1999.
[19] J. Azaña and L. R. Chen, "Synthesis of temporal optical waveforms by fiber Bragg gratings: A new approach based on space-to-frequency-to-time mapping," *JOSA B*, vol. 19, no. 11, pp. 2758–2769, Nov. 2002.